

Material flow and void defect formation in friction stir welding of aluminium alloys

X. H. Zeng, P. Xue, D. Wang, D. R. Ni, B. L. Xiao, K. S. Wang & Z. Y. Ma

To cite this article: X. H. Zeng, P. Xue, D. Wang, D. R. Ni, B. L. Xiao, K. S. Wang & Z. Y. Ma (2018) Material flow and void defect formation in friction stir welding of aluminium alloys, Science and Technology of Welding and Joining, 23:8, 677-686, DOI: [10.1080/13621718.2018.1471844](https://doi.org/10.1080/13621718.2018.1471844)

To link to this article: <https://doi.org/10.1080/13621718.2018.1471844>



Published online: 10 May 2018.



Submit your article to this journal [↗](#)



Article views: 115



View Crossmark data [↗](#)



Citing articles: 1 View citing articles [↗](#)



Material flow and void defect formation in friction stir welding of aluminium alloys

X. H. Zeng^a, P. Xue^a, D. Wang^a, D. R. Ni^a, B. L. Xiao^a, K. S. Wang^b and Z. Y. Ma^a

^aShenyang National Laboratory for Materials Science, Institute of Metal Research, Chinese Academy of Sciences, Shenyang, People's Republic of China; ^bSchool of Metallurgical Engineering, Xi'an University of Architecture and Technology, Xi'an, People's Republic of China

ABSTRACT

An ingenious experimental programme by combining artificially thickened oxide layer as marker material and 'stop-action' welding were used to study the material flow and defect formation in friction stir welding of aluminium alloys. The results showed that material flow around the pin on the advancing side (AS) was severer than that on the retreating side (RS) and the fastest velocity of material flow in the middle stir zone (SZ) was 43.9 mm s^{-1} . Moreover, the material under the RS shoulder included extruded metal only and the material under the AS shoulder included extruded and rotated metal. Lastly, instantaneous void occurrence and insufficient inflow material were reasons for the preferential formation of void defects in the top SZ on the AS.

ARTICLE HISTORY

Received 24 January 2018
Accepted 15 April 2018

KEYWORDS

Aluminium alloys; friction stir welding; deformation; material flow; void defect

Introduction

The increasing demand for light-weight and high-strength sheet metals, such as aluminium and magnesium alloys, in the aerospace, ship manufacturing, and railroad transportation industries have attracted the attention of manufacturers toward friction stir welding (FSW) because of the high mechanical properties of FSW light alloy joints [1–3]. Compared with conventional fusion welding, FSW does not involve melting and solidification of the base materials (BM) that are joined during welding [4–6]. However, void defects (including tunnel defects) sometimes occur in FSW joints if improper parameters are used in the welding process [7,8].



Recently, there has been a consensus that inappropriate material flow is the main reason for defect formation during FSW [9–11]. Based on different flow-partitioned deformation zones, Zhang et al. [6] and Arbegast [9,12] have developed some conceptual models of material flow to describe the conditions of void defect formation. Further, Liu and Wu [13] have suggested that a time-delay feature of material flow should be considered as an inducement of tunnel defect formation. However, due to complexity and instantaneity [2,14,15], the material flow during FSW is very difficult to observe and describe, and the mechanism of the formation and elimination of void defects in FSW has not been illuminated very well.

According to many related studies, void defects always occurred in the stir zone (SZ) on the advanc-

ing side (AS) [7–9,13,16–26]. For example, Chen et al. [16] reported that void defects were observed in the top SZ on the AS. This means that the SZ on the AS is potentially the position of defect formation during FSW. However, void defects were also found to appear in the SZ on the retreating side (RS) [27]. It is important to point out that the reason for preferential formation of void defects at the SZ on the AS has not been well understood so far.

It is recognised that there are distinct material flow differences in different positions of the welds [9,12]. The unusual material flow in the SZ on the AS might be the reason for void defect formation and, thus, accurate description of material flow in this position could provide a better understanding of the void defect formation mechanism at this position.

In recent years, several studies have been conducted with the goal of understanding the material flow in different positions during FSW. Colligan [28] reported that stirred material originated from the upper portion of the pin path and other material in the weld zone was simply extruded around the RS of the pin. Liu et al. [10] reported that the distance between the deformation initiation point and the pin decreased with the increase in the cross-sectional depth. Although some related simulation studies [29,30] reported that the initially located points on the AS revolved around the pin and eventually most of them returned to the AS, the material flow in the SZ on the AS has received little attention.

CONTACT P. Xue ✉ pxue@imr.ac.cn  Shenyang National Laboratory for Materials Science, Institute of Metal Research, Chinese Academy of Sciences, 72 Wenhua Road, Shenyang 110016, People's Republic of China; Z. Y. Ma ✉ zym@imr.ac.cn  Shenyang National Laboratory for Materials Science, Institute of Metal Research, Chinese Academy of Sciences, 72 Wenhua Road, Shenyang 110016, People's Republic of China

The material velocity, reflecting the material flow intensity, during FSW plays an important role in understanding the material flow behaviour [31,32]. In recent studies, some methods have been used to investigate the material velocity during FSW. Chen et al. [16] used the distance gap between the detached shear layers to calculate the material velocity. However, this method obtained the material velocity at the back of the pin only. In addition, Morisada et al. [31,33] obtained the velocity of marker material, which was inserted into the welded workpieces at different locations to trace the material flow, using two pairs of X-ray transmission systems. Liu et al. [10] also evaluated velocity based on the deformation of marker material. As these velocities only involved information regarding marker material in workpieces, the material velocity during FSW needed further study.

In this study, a combined method of artificially thickened oxide layer as the marker material [6] and 'stop-action' welding [10,13,16,34], was used to investigate the material flow in the SZ on the AS. Meanwhile, the material velocity during FSW was studied and the collective results were used to identify the reason for void defect formation in the SZ on the AS.

Experimental procedure

The materials used in this study were 6.0-mm-thick rolled plates of 2014Al-T6 with nominal composition of Al-4.8Cu-0.6Mg-0.7Mn-0.7Fe-0.9Si (wt-%). Artificially thickened oxide layer, which was obtained using an electric discharge machine on the butt surface of 2014Al-T6, was chosen as marker material. Compared with the natural oxide layer on the aluminium plates, the artificially thickened had a larger thickness, beneficial for tracing after FSW. Compared with the conventional marker materials, the oxide layer is not only thin but also metallurgically bonded with the welded material. Thus, the artificially thickened oxide layers (hereafter called the oxide layer) in different positions of a FSW joint can be used to trace the flow information about the welded material directly.

The plates were butt welded along the rolling direction with a tool tilt angle of 2.8° using a FSW machine (China FSW Center, Beijing, China). A welding tool, as shown in Figure 1, with a concave featureless shoulder 20 mm in diameter and a conical threaded pin 8 mm in root tip diameter, 5.73 mm in length, and 1 mm in thread pitch, which was made of heat-treated tool steel, was used in this study. FSW was conducted at a constant traverse speed of 100 mm min^{-1} with different tool rotation rates of 400 and 500 rev min^{-1} and the plunge depth of the tool was 0.2 mm during FSW.

For characterising the three-dimensional position in workpieces, a coordinate system was established, as illustrated in Figure 2(a). The x , y and z directions refer to the welding direction, the perpendicular direction to

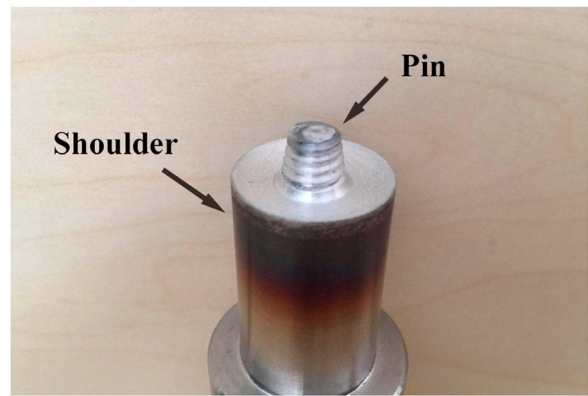


Figure 1. A welding tool used in FSW.

the welding direction from the RS to the AS, and the normal direction to the plate surface from the top to the bottom. The origin point (point O in Figure 2(a)) was the welding centre on the top surface and pin offsets from $y = -4$ to $+4 \text{ mm}$ at an interval of 1 mm were used in FSW processes of 2014Al-T6 under a tool rotation rate of 400 rev min^{-1} and a traverse speed of 100 mm min^{-1} . Schematic diagrams of the transverse cross-sections (yOz sections) of the 'offset' samples with three marked lines at different depths ($z = 1.2, 3, \text{ and } 5.7 \text{ mm}$) are shown in Figure 2(b).

At the end of the welding, the rotating tool was suddenly stopped by a brake device, leaving the tool in the workpiece, and thus utilised to 'freeze' the material flow state around the pin (Figure 2(c)), which is the so-called 'stop-action' welding. Sometimes, to facilitate the observation, after the rotating tool was suddenly stopped, the tool was withdrawn immediately. The transverse cross-sections of 'stop-action' samples at $x = 2.5, 0, \text{ and } -2.5 \text{ mm}$ were marked as sections A, B, and C, respectively (Figure 2(d)).

Metallographic observation was performed by optical microscopy (Olympus Corporation HC-300Z/OL). After grinding and polishing, the metallographic samples were etched with two reagents. One was a modified Keller's etching reagent, which included 2 mL HF, 3 mL HCl, 5 mL HNO_3 , and 190 mL H_2O . This etching reagent resulted in a high-quality image of the grain structure. The other reagent was a 2 wt-% NaOH solution, which clearly revealed the oxide layer. Some FSW joints were observed by scanning electron microscopy (SEM, FEI Quanta 600).

Results and discussion

Material flow in different positions

The transverse cross-sectional metallographs of FSW 2014Al-T6 joints, at different offset positions under 400 rev min^{-1} and 100 mm min^{-1} , showed a dark line (continuous or discontinuous) in the SZ, which was the oxide layer (Figure 3). For the RS offset FSW samples

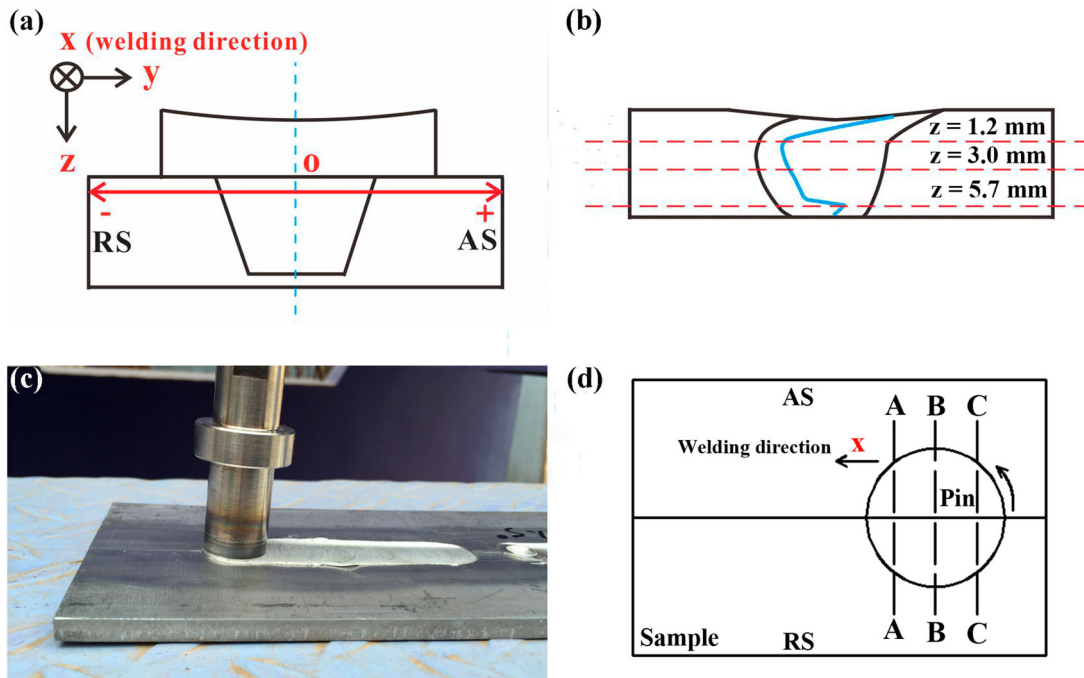


Figure 2. (a) A coordinate system, (b) the transverse cross-sections (yOz sections) of 'offset' samples with three marked lines at different depths, (c) 'stop-action' welding, and (d) position of the transverse cross-sections in 'stop-action' samples.

(Figure 3(b,d,f,h)), it was showed that the shapes of the oxide layers at the middle SZ were similar to those of the RS boundary of the SZ. The oxide layers at the top SZ moved to the AS and those at the bottom SZ did not move. The oxide layers for the RS offset FSW samples were continuous lines, which indicated that the material flow in the SZ on the RS was too weak to break the oxide layers [11].

For the AS offset FSW samples, some interesting observations were obtained for the oxide layer (Figure 3(c,e,g,i)). First, the oxide layer at $y = +1$ mm offset position was a continuous and curved line, which reflected that the material flow in this offset position was not severe. Second, at the top SZ, the oxide layers at $y = +2$ and $+3$ mm offset positions appeared to be disconnected, which indicated that material flow in these positions broke off the oxide layers and the materials were fully mixed. Third, the middle and bottom part of oxide layers at $y = +4$ mm offset position did not move and only the top part of this oxide layer was extruded by the SZ material.

Based on the results in Figure 3, some information on the material flow at different heights for various offset FSW 2014Al-T6 samples was analysed and the resultant statistics regarding oxide layers in initial positions, $z = 1.2, 3.0,$ and 5.7 mm of 'offset' samples, are shown in Figure 4(a). The symbols with different colours stand for oxide layers in different offset positions and different shapes stand for oxide layers in different heights. Due to the discontinuous top part of the oxide layers in $y = +2$ and $+3$ mm offset samples, information regarding the top part of the oxide layers for these samples was not obtained.

At $z = 1.2$ mm, only the oxide layer at $y = +4$ mm offset position moved to the AS, while oxide layers at other offset positions moved to the RS. At $z = 3.0$ mm, the oxide layer at $y = +3$ and $+4$ mm offset positions moved to the AS and those at other offset positions moved to the RS. Meanwhile, the middle part of oxide layers at $y = -1, 0, +1,$ and $+2$ mm offset positions were in close proximity. Compared with other height positions, the movements of the oxide layers at $z = 5.7$ mm were relatively small. Because the oxide layers at $y = -4, -3,$ and $+4$ mm offset positions were far away from the weld centre, these oxide layers did not move, while the oxide layers at other offset positions moved to the AS.

Figure 4(b) shows the movement distances of oxide layers in the y direction at different y and z positions. The oxide layers moved to the AS were marked by positive numbers and the layers moved to the RS were marked by negative numbers. Severe material flow led to the invisible top part of oxide layers at $y = +2$ and $+3$ mm offset positions. Thus, the movement distances in the y direction of oxide layers at these positions were defined as -4 mm.

Three important findings are revealed in Figure 4(b). First, the movement distance in the y direction decreased with increased workpiece depth. The oxide layer at $z = 5.7$ mm exhibited a short movement distance. In comparison, the movement distances of oxide layers at $z = 1.2$ and 3.0 mm were larger. Second, the oxide layers at $z = 5.7$ mm moved to the AS. In contrast, most of the oxide layers at $z = 1.2$ and 3.0 mm moved to the RS. Third, the movement distances of oxide layers in the y direction at the AS offset positions

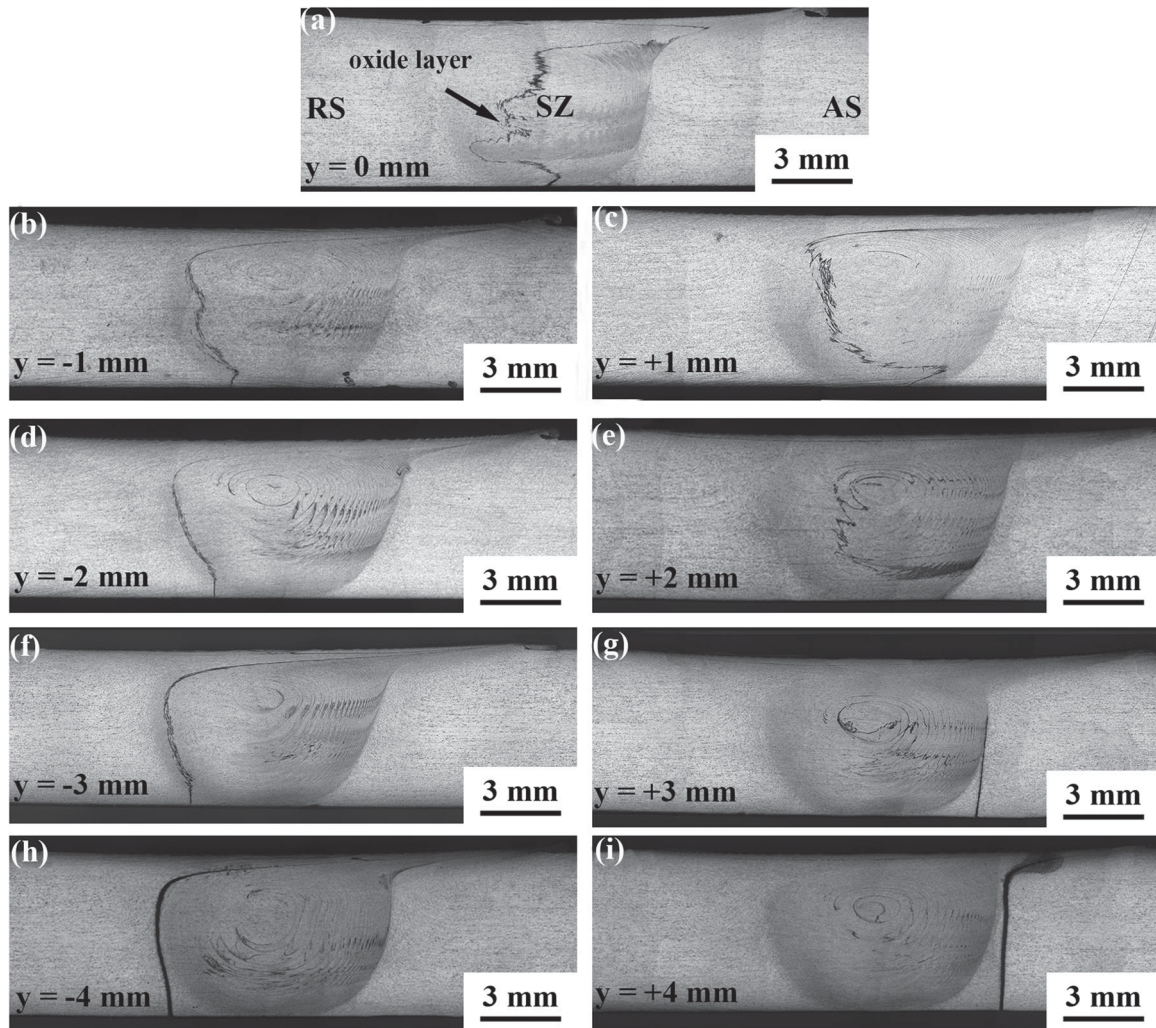


Figure 3. The transverse cross-sectional metallograph of FSW 2014Al-T6 joints at different offset positions under 400 rev min^{-1} and 100 mm min^{-1} (etched by NaOH solution).

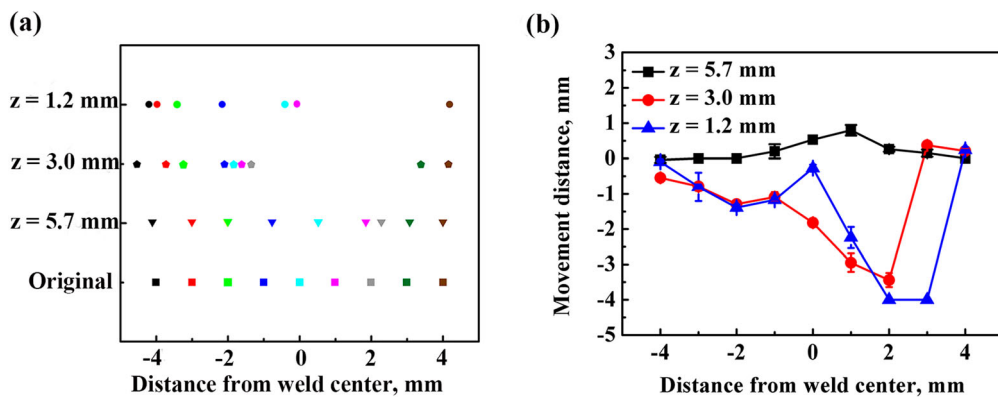


Figure 4. (a) Statistics regarding oxide layers at the initial position, $z = 1.2, 3.0,$ and 5.7 mm of 'offset' samples and (b) movement distance of oxide layer at different offsets and height positions.

were larger than those at the RS offset positions, which indicated that material flow on the AS was severer than that on the RS. Clearly, the movement distances of oxide layers in the y direction at different heights and offset positions showed that the material flow ability in the top SZ on the AS was the best during FSW.

Figure 5(a-c) shows the oxide layer distributions in the horizontal cross-sections (xOy sections) at $z = 1.2, 3,$ and 5.7 mm for $y = 0 \text{ mm}$ 'stop-action' sample, which were typical oxide layer distributions for the 'stop-action' samples. The oxide layer was observed to have rotated with the pin and finally stayed on the AS

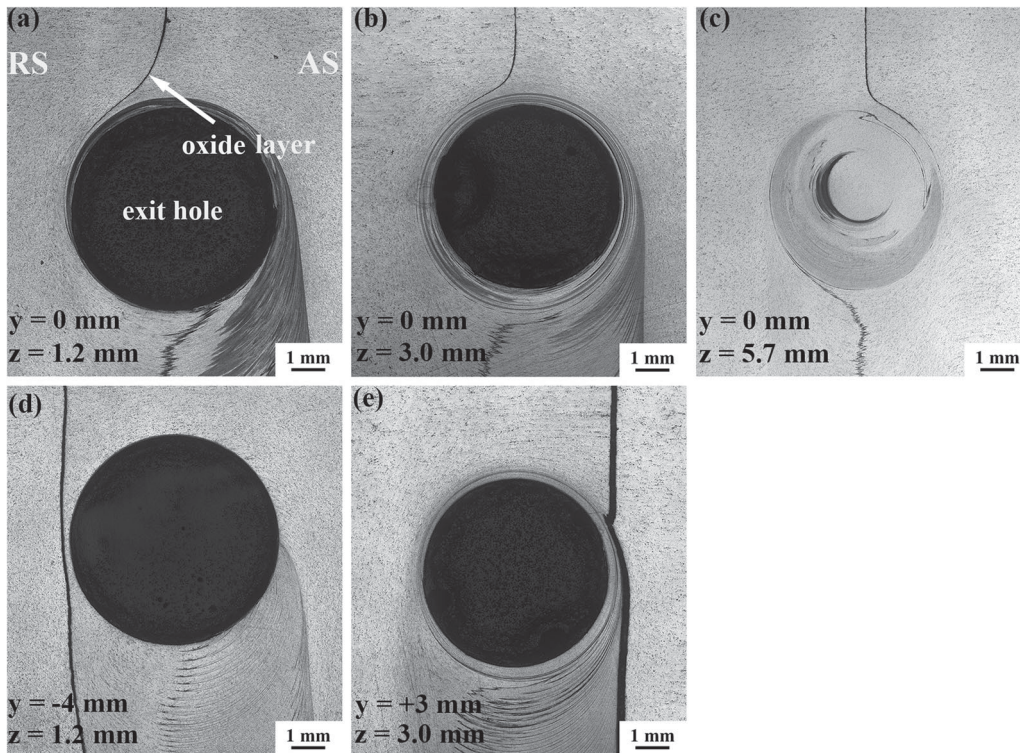


Figure 5. Oxide layer distributions in the horizontal cross-sections (xOy sections) at different offset positions in 'stop-action' samples: (a–c) oxide layer distributions in $y = 0$ mm offset position at $z = 1.2, 3.0,$ and 5.7 mm, respectively, (d) $z = 1.2$ mm of $y = -4$ mm offset position, and (e) $z = 3.0$ mm of $y = +3$ mm offset position.

or the RS. The shapes of oxide layers indicated that the material flow was continuous and laminar [13,32]. Moreover, there were two kinds of oxide layer distributions at the edges of the SZ. The first one was slight movement of the oxide layer to the AS (Figure 5(d)). The second one was the rotation of a part of the oxide layer with the pin and the extrusion of the other part by the pin (Figure 5(e)).

For further analysis, based on the results in Figure 5, schematic diagram of an oxide layer distribution in the horizontal cross-sections during FSW is showed in Figure 6(a). The distance d between the deformation initiation point on the oxide layer and the pin (exit hole) in the x direction indicated the thickness of the deformed material at the initial welding stage. The distance l between the original offset position and the oxide layer at the front end of the pin in the y direction indicated the distance of material flow at the initial stage of welding. Variations in d and l at $z = 3.0$ mm with different offset positions from $y = -2$ to $+2$ mm showed that d at the welding centre ($y = 0$ mm) was the largest (Figure 6(b)). At the same time, the d values at the RS offset positions were larger than those at the AS offset positions. However, l was observed to increase with the offset position from the RS to the AS.

Figure 6(c) shows a schematic diagram of a two-oxide layer distribution in the horizontal cross-sections during FSW. s_0 was the distance between adjacent oxide layers at the original offset positions in the y direction. In this study, s_0 was 1 mm. Then, s_1 was the distance

between adjacent oxide layers at the front end of pin in the y direction and s_2 the distance between adjacent oxide layers at the welding centre in the y direction. The material at $z = 3.0$ mm between the oxide layers at $y = 0$ and $+1$ mm offset positions was marked AS1 and that between the oxide layers at $y = 0$ and -1 mm offset position marked RS1; the rest were marked in a same manner. Variations in s_1 and s_2 at $z = 3.0$ mm with different materials from RS2 to AS2 showed that s_1 and s_2 decreased with the material from the RS to the AS (Figure 6(d)). Meanwhile, the s_1 and s_2 of RS2 were larger than those of the other materials.

Assuming the plastic aluminium alloy as incompressible, the material flow at $z = 3.0$ mm was regarded as a one-dimensional incompressible fluid flow, which met the requirements of the one-dimensional continuity equation, i.e. the volume of the fluid flowing at any two cross-sections was equal at any instance [13,29]. The continuity equation of material flow during FSW was given as $s_0 \cdot v_0 = s_1 \cdot v_1 = s_2 \cdot v_2$, where v_0 , v_1 , and v_2 are the material velocity at the initial deformation position, the front end of pin, and the welding centre, respectively. The material velocity at the initial deformation position (v_0) was the traverse speed, which was 1.67 mm s^{-1} in this study.

Variations in v_1 and v_2 with different materials from RS2 to AS2 revealed some interesting observations regarding changes of velocity (Figure 6(e)). First, v_1 and v_2 increased from the RS to the AS, which reflected that material velocities on the AS were larger than those on

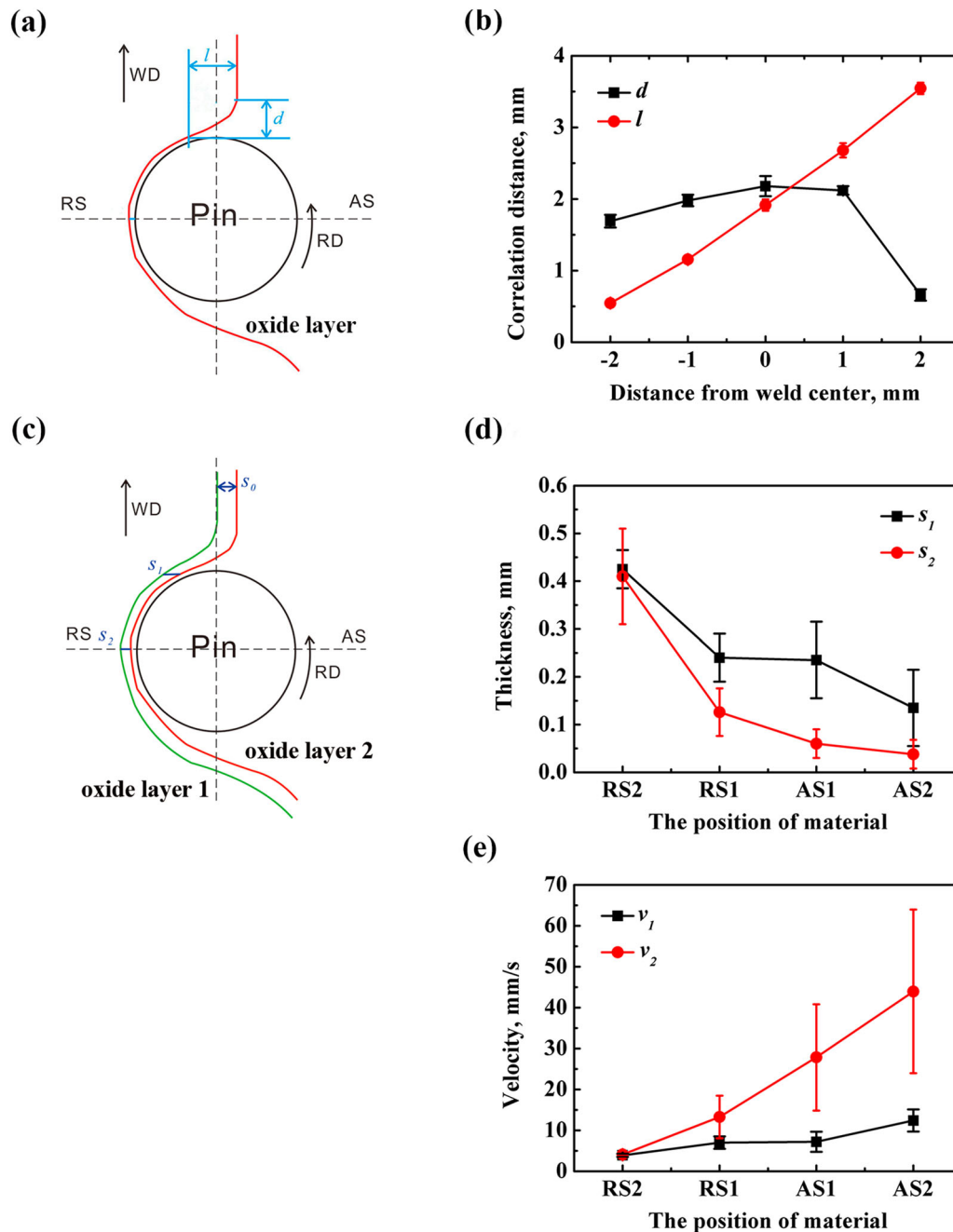


Figure 6. (a) Schematic diagram of an oxide layer distribution in the horizontal cross-sections, (b) measured values of the d and l at $z = 3.0$ mm, (c) schematic diagram of a two-oxide layer distribution in the horizontal cross-sections, (d) measured values of s_1 and s_2 at $z = 3.0$ mm, and (e) material velocity from RS2 to AS2.

the RS. Second, the gap between v_1 and v_2 of RS2 was very small and the gap between v_1 and v_2 of the material increased from the RS to the AS, which indicated that the velocities at RS2, as the material was extruded by the pin, did not change. Third, the maximum velocity of material at $z = 3.0$ mm was 43.9 mm s^{-1} , which was the v_2 of AS2 (Figure 6(e)). In contrast, the velocity of the pin edge at $z = 3.0$ mm was 136.1 mm s^{-1} , which was larger than that of material during FSW and indicated that there was relative movement between the welding tool and material. The average material velocities during FSW in other studies have been reported as $14\text{--}38 \text{ mm s}^{-1}$ [13,16,32], which are consistent with the present results.

Void defect formation in the SZ on the AS

The material flow process during FSW is further illuminated by observing the transverse cross-sections of 'stop-action' samples under 400 rev min^{-1} and 100 mm min^{-1} . Material flow details around the pin showed that there were the great differences in the material flow between the AS and the RS during FSW (Figure 7). First, the material under the AS shoulder was more than that under the RS shoulder and the space under the RS shoulder was not filled by material. According to the grain size and morphology (Figure 7(b,c)), the material under the RS shoulder included extruded metal only and the material under

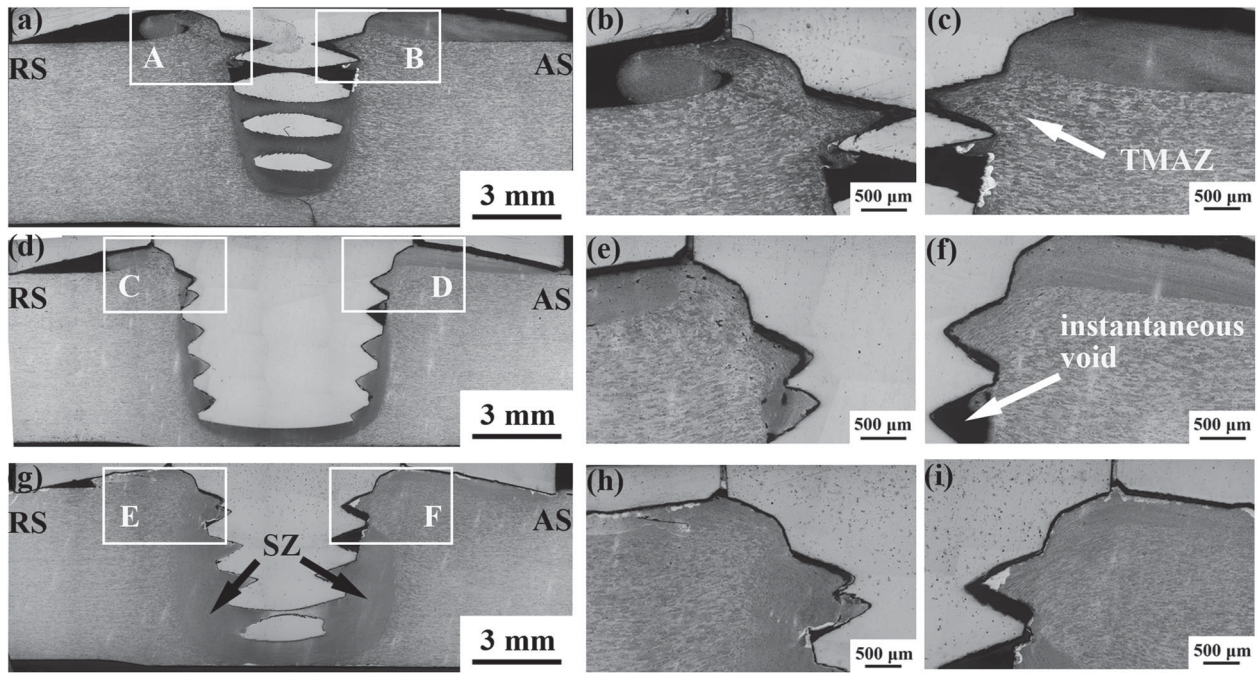


Figure 7. Transverse cross-sections of 'stop-action' FSW: (a) section A, (b) and (c) positions B and C in Figure 7(a), (d) section B, (e) and (f) positions E and F in Figure 7(d), (g) section C, and (h) and (i) positions H and I in Figure 7(g).

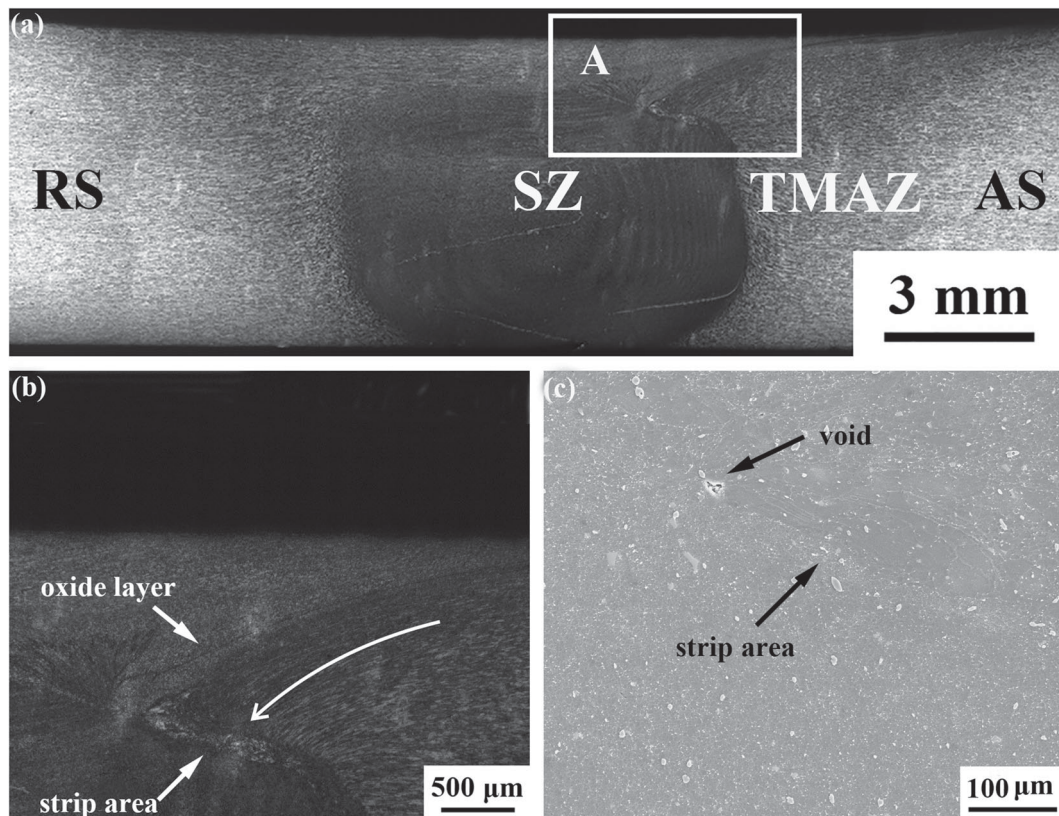


Figure 8. Transverse cross-section of FSW joints under 500 rev min^{-1} and 100 mm min^{-1} : (a) transverse cross-section of FSW joints, (b) position B, and (c) SEM micrographs of position B.

the AS shoulder included extruded and rotated metal. Second, a phenomenon involving instantaneous voids was noticed during FSW. A void that was at the triple junction of pin thread, SZ, and thermo-mechanically affected zone (TMAZ) on the AS was observed in sections B and C of 'stop-action' samples (Figure 7(d,g)).

However, defect-free FSW joints were obtained under these parameters (Figure 3(a)). This indicated that this void at the top SZ on the AS could be filled during subsequent welding process.

According to deformed grains, the material movement above the instantaneous void showed a strong

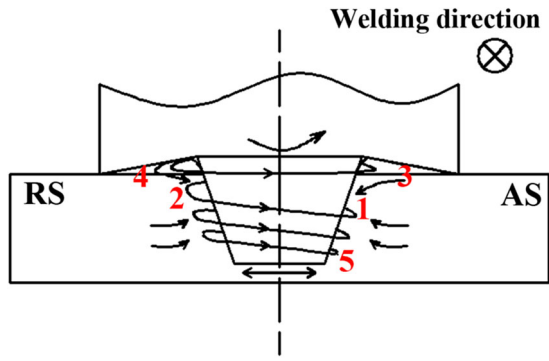


Figure 9. The schematic diagram of material flow under a low rotation rate.

downward trend (Figure 7(f,i)). Moreover, the results of ‘stop-action’ welding also showed that the material flow ability at the top SZ on the AS was the best, which led to the formation of instantaneous voids in ‘stop-action’ samples. Intuitively, the instantaneous void feature of material flow played a very pivotal role in void defect formation at the top SZ on the AS.

To identify the reason for void defect formation at the top SZ on the AS, 2014Al-T6 was welded under 500 rev min^{-1} and 100 mm min^{-1} , using a slightly increased rotation rate to promote the material flow during FSW. A strip area $\sim 1 \text{ mm}$ in length was observed on the bilateral junction of the SZ and TMAZ on the AS (Figure 8(a,b)). The strip area was a special microstructural zone with a $30 \mu\text{m}$ diameter void in the top position, as shown in Figure 8(c). Moreover, the material flow around the strip area was very complex; the morphology of deformed grains above the strip area (Figure 8(b)) was similar to that above the instantaneous void in ‘stop-action’ samples (Figure 7(d,g)). This indicated that the instantaneous void occurred during the welding process and the downward flow trend of the material above the strip area was strong. Meanwhile, the material on the RS did not move into the strip area due to the continuous oxide layer.

According to the microstructural characteristics of the strip area and the material flow around the strip area, the strip area was considered a transition state of the void defect. On the RS of the strip area, the oxide layer was continuous, so that no RS material flowed into the strip area. The instantaneous void was not filled faultlessly by the material above the strip area only. The strip area was formed to coordinate the deformation and flow of material. Thus, the preferential formation of void defects at the top SZ on the AS was attributed to instantaneous void occurrence and insufficient inflow material.

Material flow under a low rotation rate

It was noted that there was a critical total mass of material (M_T^{CR}) per cycle for a steady FSW process, moving

to the tailing side to avoid the void defects, which was originally defined by Trueba et al. [24]:

$$M_T^{CR} = \rho(\alpha \cdot \beta \cdot \phi^2)^{-1} \quad (1)$$

where ρ was the density of material, α was the pin shape factor, β was the shoulder shape factor, and the processing parameter $\phi = \omega/v$. Further, the outflow material at i position was represented by [9]:

$$M_i^{CR} = \rho \left(\alpha \cdot \beta \cdot \left(\frac{\omega_i}{v_i} \right)^2 \right)^{-1} \quad (2)$$

where ω_i was the rotation rate at each specific position, v_i was the forward travel speed, and M_{ij}^{IN} was defined as the material mass that flowed out of j position and moved into the i position. Thus, the total mass of material that flowed into i position was represented by Equation (3). Generally, a FSW process without defect met the following inequality: $M_i^{CR} \leq M_i^{IN}$.

$$M_i^{IN} = \sum M_{ij}^{IN} \quad (3)$$

Based on these results in Figure 7 and other related studies [6,19,35], the schematic of material flow during FSW under a low rotation rate is shown in Figure 9. For the AS of the SZ top (Figure 9, position 1), the total mass of material that flowed out and moved into position 1 were M_1^{CR} and M_{13}^{IN} , respectively. Abundant outflow material and less inflow material were the reason for the void defect formation at this position during FSW. With increased rotation rate, the material at the top SZ on the RS (M_{12}^{IN}) broke out of the butt surface and moved into position 1 and sufficient inflow material hindered the defect formation in this position.

Conclusions

In summary, a combined method of the artificially thickened oxide layer as the marker material and ‘stop-action’ welding was used to investigate the material flow and the defect formation in FSW of aluminium alloys. The following conclusions are reached:

- (1) the flow ability of material around the pin decreased with increased workpiece depth. Meanwhile, the material flow around the pin on the AS was severer than that on the RS and the material flow ability at the top SZ on the AS was the best during FSW;
- (2) the fastest flow velocity of material in the middle SZ was obtained, which was 43.9 mm s^{-1} . In comparison, the periphery velocity of the pin was larger than that of material flow during FSW. This indicated that there was relative movement between the welding tool and material;
- (3) the material under the AS shoulder was more than that under the RS shoulder and the space under

the RS shoulder was not filled by material. Moreover, the material under the RS shoulder included extruded metal only and the material under the AS shoulder included extruded and rotated metal;

- (4) the preferential formation of void defects at the top SZ on the AS was determined to result from instantaneous void occurrence and insufficient inflow material.

Disclosure statement

No potential conflict of interest was reported by the authors.

Funding

This work was supported by the National Natural Science Foundation of China under grant Nos. 51331008 and U1760201.

References

- [1] Hajihashemi M, Shamanian M, Niroumand B. Microstructure and mechanical properties of Al-6061-T6 alloy welded by a new hybrid FSW/SSW joining process. *Sci Technol Weld Join*. 2016;21:493–503.
- [2] Mishra RS, Ma ZY. Friction stir welding and processing. *Mater Sci Eng R*. 2005;50:1–78.
- [3] Zhao K, Liu ZY, Xiao BL, et al. Friction stir welding of carbon nanotubes reinforced Al-Cu-Mg alloy composite plates. *J Mater Sci Technol*. 2017;33:1004–1008.
- [4] Xu RZ, Ni DR, Yang Q, et al. Influence of Zn coating on friction stir spot welded magnesium-aluminum joint. *Sci Technol Weld Join*. 2017;6:512–519.
- [5] Zeng XH, Xue P, Wang D, et al. Realising equal strength welding to parent metal in precipitation-hardened Al-Mg-Si alloy via low heat input friction stir welding. *Sci Technol Weld Join*. 2018. doi:10.1080/13621718.2017.1415249.
- [6] Zhang Z, Xiao BL, Wang D, et al. Effect of Alclad layer on material flow and defect formation in friction-stir-welded 2024 aluminum alloy. *Metall Mater Trans A*. 2011;42:1717–1726.
- [7] Mahmoud TS. Surface modification of A390 hypereutectic Al-Si cast alloys using friction stir processing. *Surf Coat Tech*. 2013;228:209–220.
- [8] Zhang H, Lin SB, Wu L, et al. Defects formation procedure and mathematic model for defect free friction stir welding of magnesium alloy. *Mater Des*. 2006;27:805–809.
- [9] Arbegast WJ. A flow-partitioned deformation zone model for defect formation during friction stir welding. *Scr Mater*. 2008;58:372–376.
- [10] Liu XC, Wu CS, Padhy GK. Characterization of plastic deformation and material flow in ultrasonic vibration enhanced friction stir welding. *Scr Mater*. 2015;102:95–98.
- [11] Xu S, Deng XM. A study of texture patterns in friction stir welds. *Acta Mater*. 2008;56:1326–1341.
- [12] Arbegast WJ. Modeling friction stir joining as a metalworking process. In: Jin Z, Beaudoin A, Bieler TA, Radhakrishnan B, editor. *Hot Deformation of Aluminum Alloys III*; The Minerals, Metals and Materials Society Annual Meeting, San Diego, CA, March 2–6. Warrendale, PA: Minerals, Metals & Materials Society, 2003. p. 313–327.
- [13] Liu XC, Wu CS. Elimination of tunnel defect in ultrasonic vibration enhanced friction stir welding. *Mater Des*. 2016;90:350–358.
- [14] Heurtier P, Jones MJ, Desrayaud C, et al. Mechanical and thermal modelling of friction stir welding. *J Mater Process Tech*. 2006;171:348–357.
- [15] Mehta M, Arora A, De A, et al. Tool geometry for friction stir welding—optimum shoulder diameter. *Metall Mater Trans A*. 2011;42:2716–2722.
- [16] Chen ZW, Pasang T, Qi Y. Shear flow and formation of Nugget zone during friction stir welding of aluminium alloy 5083-O. *Mater Sci Eng A*. 2008;474:312–316.
- [17] Gerlich A, Su P, Yamamoto M, et al. Material flow and intermixing during dissimilar friction stir welding. *Sci Technol Weld Join*. 2008;13:254–264.
- [18] Kumar K, Kailas SV. The role of friction stir welding tool on material flow and weld formation. *Mater Sci Eng A*. 2008;485:367–374.
- [19] Li WY, Li JF, Zhang ZH, et al. Metal flow during friction stir welding of 7075-T651 aluminum alloy. *Exp Mech*. 2013;53:1573–1582.
- [20] Li Y, Murr LE, McClure JC. Flow visualization and residual microstructures associated with the friction-stir welding of 2024 aluminum to 6061 aluminum. *Mater Sci Eng A*. 1999;271:213–223.
- [21] Liu HJ, Zhang HJ, Yu L. Effect of welding speed on microstructures and mechanical properties of underwater friction stir welded 2219 aluminum alloy. *Mater Des*. 2011;32:1548–1553.
- [22] Mukherjee S, Ghosh AK. Flow visualization and estimation of strain and strain-rate during friction stir process. *Mater Sci Eng A*. 2010;527:5130–5135.
- [23] Palanivel R, Mathews PK, Murugan N. Optimization of process parameters to maximize ultimate tensile strength of friction stir welded dissimilar aluminum alloys using response surface methodology. *J Cent South Univ*. 2013;20:2929–2938.
- [24] Trueba L, Heredia G, Rybicki D, et al. Effect of tool shoulder features on defects and tensile properties of friction stir welded aluminum 6061-T6. *J Mater Process Tech*. 2015;219:271–277.
- [25] Zhang Z, Xiao BL, Ma ZY. Influence of water cooling on microstructure and mechanical properties of friction stir welded 2014Al-T6 joints. *Mater Sci Eng A*. 2014;614:6–15.
- [26] Zhao YH, Lin SB, Wu L, et al. The influence of pin geometry on bonding and mechanical properties in friction stir weld 2014 Al alloy. *Mater Lett*. 2005;59:2948–2952.
- [27] Balasubramanian V. Relationship between base metal properties and friction stir welding process parameters. *Mater Sci Eng A*. 2008;480:397–403.
- [28] Colligan K. Material flow behavior during friction stir welding of aluminum. *Weld J*. 1999;78:229–237.
- [29] Kadian AK, Biswas P. A comparative study of material flow behavior in friction stir welding using laminar and turbulent models. *J Mater Eng Perform*. 2015;24:4119–4127.
- [30] Pashazadeh H, Teimournezhad J, Masoumi A. Numerical investigation on the mechanical, thermal, metallurgical and material flow characteristics in friction stir welding of copper sheets with experimental verification. *Mater Des*. 2014;55:619–632.
- [31] Morisada Y, Fujii H, Kawahito Y, et al. Three-dimensional visualization of material flow during friction stir welding by two pairs of X-ray transmission systems. *Scr Mater*. 2011;65:1085–1088.

- [32] Schmidt HNB, Dickerson TL, Hattel JH. Material flow in butt friction stir welds in AA2024-T3. *Acta Mater.* [2006](#);54:1199–1209.
- [33] Morisada Y, Imaizumi T, Fujii H. Clarification of material flow and defect formation during friction stir welding. *Sci Technol Weld Join.* [2015](#);20:130–137.
- [34] Prangnell PB, Heason CP. Grain structure formation during friction stir welding observed by the ‘stop action technique’. *Acta Mater.* [2005](#);53:3179–3192.
- [35] Shi L, Wu CS, Liu HJ. Modeling the material flow and heat transfer in reverse dual-rotation friction stir welding. *J Mater Eng Perform.* [2014](#);23:2918–2929.